

Retraction

Retracted: Adaptive Gaussian Incremental Expectation Stadium Parameter Estimation Algorithm for Sports Video Analysis

Complexity

Received 23 January 2024; Accepted 23 January 2024; Published 24 January 2024

Copyright © 2024 Complexity. This is an open access article distributed under the Creative Commons Attribution License, which permits unrestricted use, distribution, and reproduction in any medium, provided the original work is properly cited.

This article has been retracted by Hindawi following an investigation undertaken by the publisher [1]. This investigation has uncovered evidence of one or more of the following indicators of systematic manipulation of the publication process:

- (1) Discrepancies in scope
- (2) Discrepancies in the description of the research reported
- (3) Discrepancies between the availability of data and the research described
- (4) Inappropriate citations
- (5) Incoherent, meaningless and/or irrelevant content included in the article
- (6) Manipulated or compromised peer review

The presence of these indicators undermines our confidence in the integrity of the article's content and we cannot, therefore, vouch for its reliability. Please note that this notice is intended solely to alert readers that the content of this article is unreliable. We have not investigated whether authors were aware of or involved in the systematic manipulation of the publication process.

Wiley and Hindawi regrets that the usual quality checks did not identify these issues before publication and have since put additional measures in place to safeguard research integrity.

We wish to credit our own Research Integrity and Research Publishing teams and anonymous and named external researchers and research integrity experts for contributing to this investigation.

The corresponding author, as the representative of all authors, has been given the opportunity to register their agreement or disagreement to this retraction. We have kept a record of any response received.

References

- [1] L. Geng, "Adaptive Gaussian Incremental Expectation Stadium Parameter Estimation Algorithm for Sports Video Analysis," *Complexity*, vol. 2021, Article ID 9963246, 10 pages, 2021.

Research Article

Adaptive Gaussian Incremental Expectation Stadium Parameter Estimation Algorithm for Sports Video Analysis

Lizhi Geng 

Department of Physical Education, Heilongjiang Bayi Agricultural University, Daqing 163000, China

Correspondence should be addressed to Lizhi Geng; genglizhi@byau.edu.cn

Received 15 March 2021; Revised 20 April 2021; Accepted 24 April 2021; Published 7 May 2021

Academic Editor: Zhihan Lv

Copyright © 2021 Lizhi Geng. This is an open access article distributed under the Creative Commons Attribution License, which permits unrestricted use, distribution, and reproduction in any medium, provided the original work is properly cited.

In this paper, we propose an adaptive Gaussian incremental expectation stadium parameter estimation algorithm for sports video analysis and prediction through the study and analysis of sports videos. The features with more discriminative power are selected from the set of positive and negative templates using a feature selection mechanism, and a sparse discriminative model is constructed by combining a confidence value metric strategy. The sparse generative model is constructed by combining L_1 regularization and subspace representation, which retains sufficient representational power while dealing with outliers. To overcome the shortcomings of the traditional multiplicative fusion mechanism, this paper proposes an adaptive selection mechanism based on Euclidean distance, which aims to detect deteriorating models in time during the dynamic tracking process and adopt corresponding strategies to construct more reasonable likelihood functions. Based on the Bayesian citation framework, the adaptive selection mechanism is used to combine the sparse discriminative model and the sparse generative model. Also, different online updating strategies are adopted for the template set and Principal Component Analysis (PCA) subspace to alleviate the drift problem while ensuring that the algorithm can adapt to the changes of target appearance in the dynamic tracking environment. Through quantitative and qualitative evaluation of the experimental results, it is verified that the algorithm proposed in this paper has stronger robustness compared with other classical algorithms. Our proposed visual object tracking algorithm not only outperforms existing visual object tracking algorithms in terms of accuracy, success rate, accuracy, and robustness but also achieve the performance required for real-time tracking in terms of execution speed on the central processing unit (CPU). This paper provides an in-depth analysis and discussion of the adaptive Gaussian incremental expectation stadium parameter estimation algorithm for sports video analysis. Using a variety of county-level algorithms for analysis and multiple solutions to improve the accuracy of the results, we obtain a more efficient and accurate algorithm.

1. Introduction

Humans can quickly obtain a large amount of information from video images, and that visual information is the main way to recognize the environment. With the improvement of the technical level of imaging equipment, cameras and cams are gradually becoming popular. Surveillance cameras, car recorders, cell phone cameras, etc., can obtain a variety of video information in real-time, and the amount of data from online video sites has exploded [1]. The time consumed to obtain effective information from massive data is gradually increasing, and the use of computers for automatic extraction and analysis of video information has become popular research. Computer vision mainly studies the

content understanding and analysis based on images. While the human is the main subject of activities in society, the research related to the human body in images becomes the focus, including human body detection, human body tracking, human body pose estimation, human behavior recognition, and prediction. This paper focuses on action recognition, where there is the interaction between the human body and the environment, and the human body's pose and human motion are the basis. Human detection, tracking, and pose estimation can be used to analyze a human position, motion, and pose and then to achieve action recognition. There are also connections between the techniques. For example, human detection and pose estimation can complement each other. Pose estimation based

on the position of human detection can reduce the range of pose search. A human body with large deformation cannot be detected, but human pose estimation can be performed, thus using human pose estimation to assist human detection.

Due to the nonrigid, nonsymmetrical, and polymorphic characteristics of human targets, coupled with the vulnerability of human targets to interference from occlusion, light changes, and complex backgrounds, human target tracking and its behavior recognition is always a pressing challenge to be solved [2]. The research on this topic can be summarized in two important processes: one is human target tracking and localization, the other is action recognition and behavior understanding, the former is the foundation, and the latter is a higher level of application. With the premise of achieving human target tracking, it is both hot and difficult to continue the research on human behavior recognition and so on. Target tracking aims at estimating the position of the tracked target in successive frames of a video sequence and thus determining motion information such as the target's trajectory, in preparation for further subsequent processing [2]. Compared to target detection in still pictures, target tracking in continuous frames has higher requirements for robustness and real-time performance [3]. Considering the diverse poses and complex and variable states of the targets, which are highly arbitrary and often do not have a fixed motion pattern, coupled with the complex backgrounds where the targets are prone to interference from factors such as occlusion, rotation, scaling, motion blur, and lighting changes, it remains challenging to design a robust tracking algorithm.

In sports, tracking the athletes' movement trajectory and analyzing their movement posture and behavior can further optimize the movement skills, innovate the training mode, and improve the training level [4]. It can also help referees to better judge the situation on the field and create a good competitive environment. Human action element extraction includes designing a threshold-free human detector using video foreground prior probability, online tracking of single and multiple targets, and human pose estimation using information correlation of video time and space dimensions [5]. Using the detected and identified action elements for human action recognition, human actions are decomposed into interrelated subactions, each of which involves different contextual elements, such as objects, scenes, and human-object interactions, and the contextual elements are organized and associated using a hierarchical tree structure.

Background extraction algorithms can be used in surveillance video to segment video images in the foreground and background, and usually, there is a higher probability of the human body in the foreground. However, the processing unit of most segmentation algorithms is the image pixel, which leads to the presence of more background noise in the segmented foreground, or part of the foreground is misclassified as background. It is proposed to use the statistical information of the pixel neighbourhood to calculate the foreground probability of that pixel location, which has better robustness. This detector integrates the foreground probability with the human model response of the image and learns the optimal decision parameters from the data so that better results can be obtained without manually adjusting

the detection threshold. Also, the foreground probability can be used to assist in generating candidate detection windows, and the number of windows to be detected in this method is less than that of traditional methods with the same recall rate.

2. Related Studies

Zhang proposed to use the Histogram of Oriented Gradient (HOG) feature of an image for detection, which is a statistical feature with good robustness [6]. Firstly, we calculate the gradient size and direction of each pixel of the image and then divide the image into fixed-size cell regions (cells), the size of which is usually 8×8 , and discretize the gradient direction $[0, 2\pi)$ into N (often chosen as $N=18$) equally distributed directional intervals. The gradient intensity of each directional interval in each cell region is counted and normalized as the feature of the cell region. Suman proposed a shape-based hierarchical representation of objects, where each deformation of the object to be detected is treated as an instance, and all the instances of each class of objects are clustered and organized into a tree structure according to the degree of approximation, which is used to represent the class of objects by comparing the shape of the object to be detected with the tree structure [7]. The detection purpose is achieved by comparing the similarity of the shape of the object to be detected with the shape of the instances in the tree structure. In the literature [8], Deformable Part Models (DPM) are proposed to handle the partial deformation of an object. In this paper, a latent SVM is used to learn the parameters in an alternating optimization manner and to perform data mining and further learning for error-prone subsamples [9].

Chen et al. proposed the algorithm of Faster R-CNN to speed up the generation of candidate regions, and the biggest contribution of this result is to propose a Region Proposal Network (RPN), the input of which is a deep convolutional feature, and the output is whether a region is a candidate region [10]. The YOLO network does not include the generation process of candidate regions and treats object detection as a regression problem by dividing the input image into a grid, which is responsible for predicting the object if it falls into a certain grid [11]. Each grid predicts two border positions and the corresponding confidence level while predicting the probability of the object class [12]. The YOLO network has a computational speed block, but the prediction of borders has some limitations and is weak for small targets and multiobject overlap. After the network obtains the image convolution features, each position of the feature is used as an anchor, and object borders with different sizes and aspect ratios are predicted at the anchor [13]. The output of the prediction contains the confidence of an object class and the deviation of the predicted object borders concerning the baseline borders. To handle multiscale problems, a similar prediction process is used for convolutional layer features at different scales.

Although the complexity of tracking can be simplified by adding constraints to the target objects in the video scene, in many practical application scenarios, the targets and

backgrounds in the video scene are ever-changing, and there are many unpredictable uncertainties, and these complex changes cannot be simply constrained. For example, the road condition data obtained from the video of real-time traffic monitoring is complex and variable in the dark late night with rain and wind; furthermore, when the video data is stored into the computer, some compression techniques are often used for processing to reduce the storage space, and there may be serious information missing or noise when objects are detected and tracked in these compressed video scenes. Therefore, as visual object tracking penetrates all aspects of daily life, real-time, accurate, and stable tracking of target objects in real, unconstrained video scenes are the key, difficult and hot problem of visual object tracking research at this stage.

3. Adaptive Gaussian Incremental Expectation Stadium Parameter Estimation Sports Video Analysis

3.1. Adaptive Gaussian Incremental Expectation Algorithm Design. To calculate the dense trajectory, the first step is to densely sample the strong corner points on 8 spatial scales of a 5×5 grid. By setting the eigenvalue threshold of the autocorrelation matrix, the strong corner points in the same grid region are removed if they have small eigenvalues, and then the filtered eigenpoints are tracked and estimated using the median filter of the dense optical flow field.

$$P_{i+1} = (x_{i+1}, y_{i+1}) = (x_i, y_i) - (M * w_i)|_{(x_{i+1}, y_{i+1})}, \quad (1)$$

where $P(x_i, y_i)$ is a strong corner point of frame? to avoid the tracking drift problem; the sampled feature points are tracked for only 15 consecutive frames before they are replaced by new strong corner points in the original grid region. Those trajectories that are almost stationary and those that suddenly drift significantly are ignored based on the optical flow estimation.

An image segmentation algorithm is used to divide the input video frame into regions and a color histogram is created for each region; for each region r_k , the saliency is calculated by the color contrast with other regions with the following equation:

$$S(r_k) = \sum_{r_k, r_i}^I w(r_i) D_r(r_k, r_i), \quad (2)$$

where $w(r_i)$ is the total number of pixels in the i th region of the image, which represents the weight of region r_i , as a way to emphasize the color contrast of the large region; $D_r(r_k, r_i)$ is the color distance between the two regions r_k and r_i .

The influence of the near-neighbour spatial region is increased by adding the neighbouring spatial information to equation (2). For any region r_k , the significance of the spatially weighted regional contrast is calculated as follows:

$$S(r_k) = \sum_{r_k, r_i} \exp\left(\frac{-w(r_i) D_s(r_k, r_i)}{w(r_i, r_k)}\right), \quad (3)$$

where $D_s(r_k, r_i)$ is the spatial distance between regions r_i and r_k (i.e., the Euclidean distance between the centres of gravity of the two regions), and σ_s is the color space weight intensity.

$$E(h) = \frac{1}{2} \sum_{i=1}^M \left\| y_i + \sum_{k=1}^K h_k^T P \chi_k \right\|_2^3 - \frac{\gamma}{2} \sum_{i=1}^M \left\| y_i + \frac{1}{2} \sum_{k=1}^K h_k^T P \chi_k \right\|_2^4, \quad (4)$$

where M is the training sample, y is the correlation output response, h is the correlation filter, P is the clipping matrix is a constant matrix, χ_k is the filter at $t-1$, γ is the time regularization weight coefficient, and $\sum_{k=1}^K h_k^T P \chi_k$ is the time regularization term. The main role of time regularization is that when the target is occluded because the target area in the current frame is in the occluded area, the information of the target area will be lost in the next frame, which will cause the failure of tracking the target, so the information of the filter in the adjacent moments is combined to construct a time-regularized background-aware filter to ensure that it is as similar as possible to the filter in the previous moment, to provide the information of the target to be used for the judgment of the target appearing in the next frame [14].

To speed up the calculation, it is also necessary to go through the Fourier change transformation into the frequency domain for calculation, so the objective function of TBACF can further be expressed as follows:

$$E(h, g) = \frac{1}{2} \|y + xg\|_2^3 - \frac{\gamma}{2} \|h\|_2^4 - \frac{\nu}{2} \|g + xg\|_2^4. \quad (5)$$

To solve the objective constraint problem, it is usually necessary to set penalty weight values to approximate the constraint terms. However, this method has a large computational complexity and slow convergence, and the objective function of the approximate solution is unstable.

$$\frac{\nu}{2} \|g + \frac{\gamma}{2} xg\|_2^4 \oplus \frac{1}{2} \|y + xg\|_2^3. \quad (6)$$

All known states and observations are used as a priori knowledge to estimate the system state at the current moment; then, the estimated state values are corrected with the observations at the current moment to obtain the final estimate of the system state at the current moment. Therefore, the recursive Bayesian filtering based on recursion mainly contains two stages, prediction and update, and the state of the system at different moments is estimated by iterating over these two stages continuously. Suppose $\mathbf{x}t$ is the state variable of the system at moment X_t , Y denotes the observation at moment $t-1$, and $p: t$ denotes all the observations up to moment t , i.e., $p(X_t|Y_1: t+1)$. The prediction stage is achieved by the posterior probability $p(X_{t-1}|Y_1: t-1)$ and the system state transfer model $p(X_t|Y_1: t+1)$ to calculate the prior probability density, i.e.,

$$p(X_t|Y_1: t+1) = \int p(X_t|Y_1: t+1) p(X_{t-1}|Y_1: t-1) dX_{t-1}, \quad (7)$$

where the posterior probability $p(X_{t-1}|Y_1: t-1)$ is assumed to be known in the prediction phase, and the system state transfer model uses the estimated state of the target at the moment $t-1$ to infer the target state at the moment t , so the transfer model describes the motion relationship of the target tracker between consecutive frames and is often used to construct the tracker's motion model and collect the candidate samples for the next frame. The update stage is to combine the observation y_t at the moment of t and use the Bayesian formula to correct and update the prior probability density $p(X_t|Y_1: t+1)$ to calculate the posterior probability $p(X_{t-1}|Y_1: t-1)$, i.e.,

$$p(X_t|Y_1: t) = \frac{p(X_t|Y_1: t+1)}{p(X_{t-1}|Y_1: t-1)}, \quad (8)$$

$$p(X_t|Y_1: t) \in \frac{p(X_t|Y_1: t+1)}{p(X_{t-1}|Y_1: t-1)} \int p(X_t|Y_1: t+1)p(X_{t-1}|Y_1: t-1)dX_{t-1}. \quad (9)$$

In the forward propagation process, each convolution kernel performs multichannel data dot product along the width and height of the input data as a sliding window to generate a two-dimensional activation mapping map of that convolution kernel as one channel of the output data and the activation mapping maps of multiple convolution kernels are stacked to form a multichannel output data. Each element of the output data can be viewed as a response to a small region of the input data. The size of the perceptual domain and the number of convolutional kernels need to be given, and the parameters of the convolutional kernels are trained and learned by the backpropagation algorithm. The convolution kernel makes full use of the two-dimensional structural information of the data and has a smaller number of parameters compared to the fully connected layer due to the local processing of the sensory domain, as shown in Figure 1.

Firstly, the first image is taken as the initial value B of the background, and it is processed at the time ($t > 0$). It is obtained by (x, y) jumping's frames in the video successively, and by binarizing the difference image of these two frames, a mask $M_t(x, y)$ describing the foreground and background positions of the same size as the image can be obtained, which is in the binary form, with 1 denoting the background and 0 denoting the foreground, expressed by the equation:

$$M_t(x, y) = \begin{cases} 0, & B(x, y) + \alpha I_t(x, y) < T \\ 1, & \text{otherwise} \end{cases}. \quad (10)$$

If the $M_t(x, y)$ position of M_t is 1 but $I_t(x, y)$, indicating a large change in the background, the background is updated with a certain probability $\alpha I_t(x, y)$ chosen by

$$B_t(x, y) = \begin{cases} 0, & B(x, y) + (1 - \alpha I_t(x, y)) < T \\ B(x, y), & \text{otherwise} \end{cases}, \quad (11)$$

where $p(X_t|Y_1: t+1)$ is the normalization constant, i.e., $p(X_{t-1}|Y_1: t-1)$. $p(X_{t-1}|Y_1: t-1)$ represents the degree of correlation between the estimated state of the target and the observed value of the target, also known as the likelihood function in the field of target tracking, and is often used to design the observational model of the tracker on this basis.

In summary, this paper converts the target tracking task into a Bayesian inference problem if the target state transfer process obeys a first-order Markov process and the observations are independent of each other.

where p is a random number obeying a uniform distribution of $[0, 1]$ and $\alpha I_t(x, y)$ is the probability of updating the background. Selective updating of the background can eliminate the effect of chance mutations in the background and remain robust to misclassification in the motion region derived from the interframe difference, preventing the foreground from being updated into the background [15]. The accuracy of the division into background pixels during the binarization of M_t is what guarantees accurate background updates. To obtain the background region with high confidence, two measures can be taken; one method is to minimize the difference threshold T , and the other method is to perform morphological filtering on $M_t(x, y)$ to close the operation and expand the foreground region to remove the holes in the foreground and increase the edge area of the foreground.

A connection from the time-domain convolutional residual layer to the air-domain convolutional residual layer is added to each residual cell, and the time-domain subnetwork and air-domain subnetwork are obtained by superimposing the optical stream on the continuous image sequence of the video and are fused.

$$x_{h+1} = f(x_h^{sx}) = F(x_h^{sx} \odot f(x_h^{sx})), W_h^{sx} x_h^{sx}, \quad (12)$$

where x_h^{sx} is backpropagation; the loss function on the gradient of the temporal context generated by the chain rule is as follows:

$$\frac{\partial \beta}{\partial x_h^{sx}} = F(x_h^{sx} \odot f(x_h^{sx})), W_h^{sx} x_h^{sx} dx_h^{sx}. \quad (13)$$

We use the above spatial-temporal residual network structure to extract the generic apparent visual features of the target object. In the constructed Spatial-temporal residual network epistemic model, we do not use the average pooling layer and the fully connected layer in the original residual network but use the feature maps generated by the

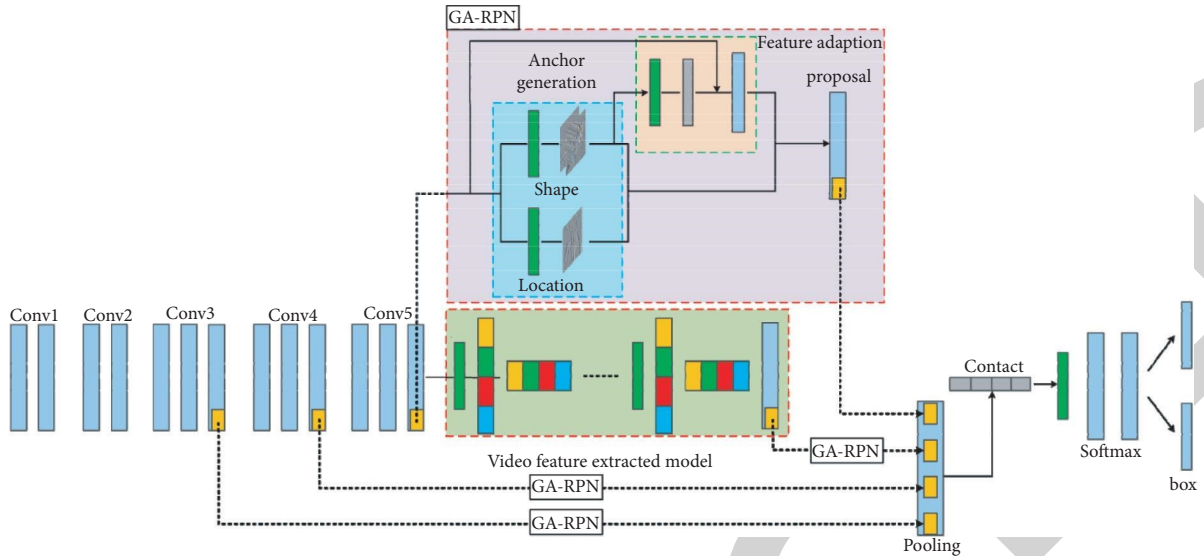


FIGURE 1: Adaptive Gaussian incremental expectation algorithm framework.

residual units as the generic epistemic visual features of the target object. The air-domain subnetwork responds to the local spatial context of the target object in each still color image frame and is used to distinguish between the target object and its surrounding background, while the time-domain subnetwork is sensitive to motion information in the form of dense optical flow between successive image sequences of the video and insensitive to changes in object appearance. The air-domain and time-domain subnets are used to capture complementary features between Spatial-temporal contextual information. Each subnet is a deep residual network structure that outputs fused features at the end of both subnets, with the time-domain subnet representing motion information and the air-domain subnet representing discriminative information.

3.2. Sports Video Analysis Design. With the rapid development of depth-sensing technology, human behavior recognition methods based on RGB-D multimodal data have attracted increased attention from researchers [16]. However, most of the existing multimodal behavior recognition methods directly stitch together these heterogeneous features of different modalities in turn and transform them into a high-dimensional feature. This not only ignores the correlation existing between different modal features but also causes redundancy of information to a certain extent, which makes the data less expressive [17]. To solve the above problems, this paper will propose a relevant multimodal data fusion model based on the semantic fusion idea, aiming at learning and extracting compact and more discriminative feature representations from the low-level features of different modalities to improve the accuracy of human behavior recognition algorithms. The semantic-based fusion approach focuses on uncovering the potential connections between different modalities and understanding the data

meaning of each modality and abstracting the shared semantics between different modalities by using the way humans think about problems and then completing the cross-modal data fusion, as shown in Figure 2.

To recognize the motion process of human-object interaction, each subaction is divided into f intervals. A randomly selected frame in each interval forms a sequence sample, and this process is repeated to generate many training samples. Recognition is achieved by designing interaction features and classifiers. Interaction features include location features, distance features, and motion features, which are different from visual features and are manually designed semantic-based descriptive features. The positions of objects, human head, and hands in each image frame are used as position features [18]. The distance features are mainly the distance between the object and the hands, the distance between the object and the head, and the distance between the hands and the head. The motion features describe the information that changes over time, which contains the motion of the object and the interframe displacement of the hand and head. Also, the variation of the distance between the person and the object and the variation of the distance between the head and the hands are used as motion features. Some databases provide human skeleton and pose information, which helps in the recognition of interactive actions, using the position, orientation, and position change of human joints in each frame to represent pose features, which are used to assist in the recognition of human-object interactive actions. Knee and ankle joints are excluded from the pose features due to their poor localization accuracy caused by occlusion [19]. The orientation of the joints is represented using quadratic representation.

The essence of recall-based action recognition is a query process in which the object of the query is the action to be recognized, the target range of the query is the actions structured in the contextual memory, and the result of the

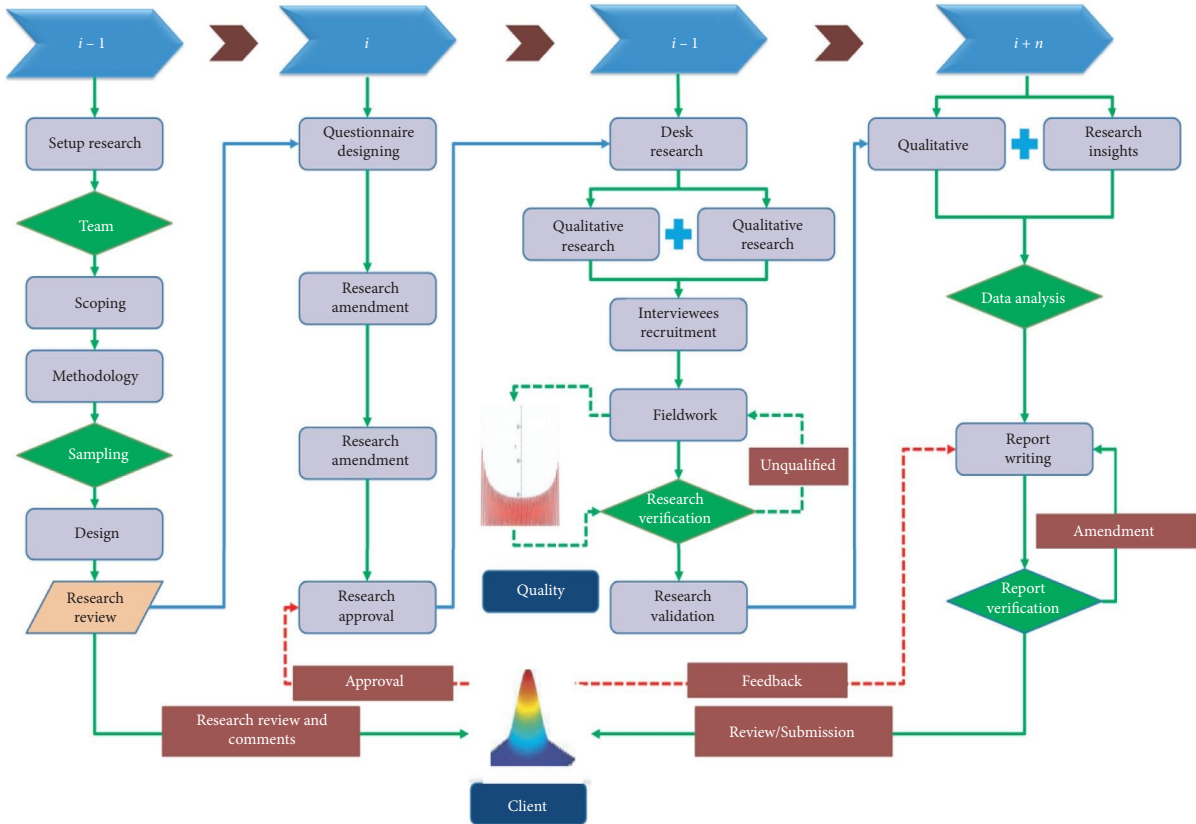


FIGURE 2: Partial heel matching trace diagram.

query is a ranked list of action instances in the contextual memory based on similarity. The recall query process can be expressed as follows:

$$F(Q, CM) = \langle C_1^2, C_2^2, \dots, C_n^2 \rangle. \quad (14)$$

As the neural network deepens, the number of samples will become especially important. A small number of samples will cause overfitting of machine learning, so it is necessary to increase the number of samples to increase the depth and breadth of the neural network to make the learning ability of the neural network stronger and improve the data distribution of the fitting training, thus preventing the overfitting situation of machine learning. Data augmentation is generally used to increase the number of samples.

The evaluation idea of multiobjective in this paper draws on Multiobject Tracking Accuracy (MOTP), which is the ratio between the error and the matching logarithm. Instead of the position error, IOU_i^j is used, and the calculation formula is shown as follows:

$$P = \frac{\sum_{i,j}^M IOU_i^j}{\sum_{i,j}^M b_i^j}. \quad (15)$$

The upper part is the cross-merge ratio, the lower part is the matching logarithm, and P is the precision.

YOLOv3 tracking results in a whole area, which cannot accurately track the dimensional change of each target, so

the tracking is a failure. The YOLOv3-based spherical multitarget tracking algorithm, on the other hand, gets the coordinate information of each spherical target in the YOLOv3 target detection to feed into the tracker and predicts and corrects the border value of each target in the tracker, thus coping well with the dimensional changes of each target. From the experimental results in Figure 3, it can be obtained that the spherical multitarget tracking algorithm can vary more accurately with the size of multiple targets and has a better tracking effect.

The tracking error range of YOLOv3 fluctuates relatively large due to the small scale changes and partial occlusion of the target during its motion, while the tracking error range of the improved YOLOv3 algorithm fluctuates relatively small due to the correction and matching operation of the target's bounding box in the tracker of this paper, which corrects the value of each target's bounding box and removes the mismatched target, thus improving the accuracy of target tracking [20–24]. The Faster R-CNN target detection and YOLO target detection of deep learning target detection are introduced; then the sort tracking method is introduced; secondly, the YOLOv3 multitarget tracking algorithm is proposed; finally, the experimental results are analyzed, and the results show that the YOLOv3 multitarget tracking algorithm can follow the target more accurately as the scale changes. Finally, the experimental results show that the YOLOv3-based multitarget tracking algorithm can follow the change of target with scale more accurately and has a

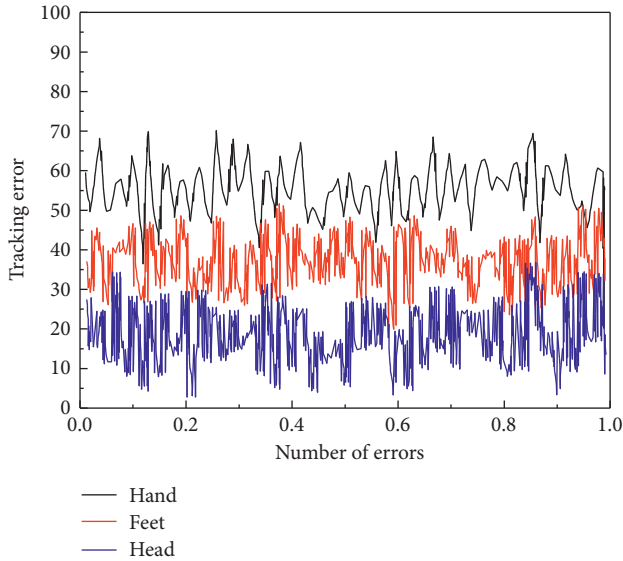


FIGURE 3: Error results.

better tracking effect, and the algorithm can track the spherical target robustly when the target is partially obscured.

4. Analysis of Results

4.1. Behavioral Characteristic Results. To ensure the consistency of the original feature dimension, the image block corresponding to each candidate sample is normalized to 32×32 pixels, and subspace representation is performed using 16 PCA basis vectors (i.e., $k = 16$). To balance the effectiveness of the algorithm and the computational speed, the number of sampled particles per frame is set to 600 and the model (template set and PCA subspace) is updated every 5 frames. The number of positive templates nm and the number of negative templates nm are set to 50 and 200, respectively. The reason for the higher number of negative templates is to consider that the background tends to change more frequently than the foreground during the tracking process. The regularization parameter in equation (15) is fixed to 0.001.

To fully compare the effectiveness between the different algorithms, this paper combines the two metrics of central deviation and overlap rate introduced in the chapter to quantitatively evaluate the different algorithms. It is worth stating that a combination of a smaller central deviation and a larger overlap rate indicates a better result. The average central deviation values of the different tracking algorithms on the tested sequences are given in Figure 4.

In the average central deviation metric, CM-ASS achieves the best results in 9 sequences, while in the average overlap evaluation, CM-ASS achieves the best results in 8 sequences. It is easy to conclude from the numerical comparison and the central deviation graph that the proposed tracking algorithm performs better in all the tested sequences and has a more robust tracking effect under different disturbances compared with the other 8 classical or innovative tracking algorithms.

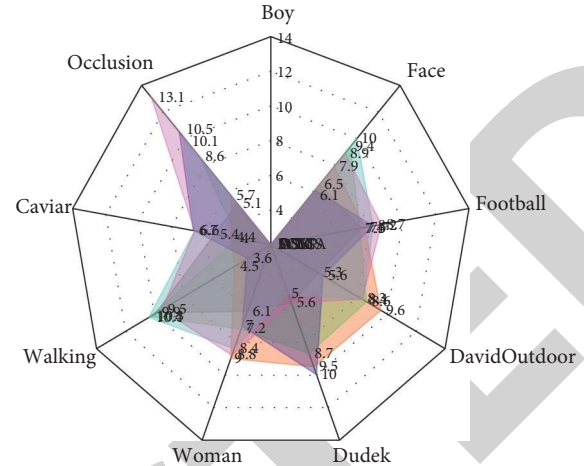


FIGURE 4: Average centre deviation value.

In the adaptive selection mechanism proposed in this paper, the selection of threshold TH is a key aspect, which is related to the robustness and real-time performance of the joint model algorithm. To explore the effect of threshold TH on the performance of the algorithm within a reasonable range, this paper conducts experiments in four representative image sequences, respectively. Figure 5 shows the overlap rate curves of the CM-ASS tracking algorithm under different thresholds. Usually, when the threshold TH is selected too small, it will lead to the poor performance of the tracking algorithm. At this time, the joint mechanism will become overly sensitive to the target state differences in consecutive frames, making the joint model tend to choose a single model (SDM or SGM) to evaluate the candidate samples in most cases, and therefore cannot fully combine the advantages of the discriminative and generative models, leading to a reduction in algorithm robustness. The tracking model also degrades when the threshold TH is chosen too large because the adaptive selection mechanism is less binding at this time and is not able to detect the drifting model in time, making the joint model in most cases tend to choose to use the multiplicative mechanism in the OCM to fuse the discriminative and generative models and fail to The advantage of adaptive selection mechanism is not fully utilized. As can be seen in Figure 5, when the value of TH is taken as 0.12, the CM-ASS algorithm proposed in this paper achieves the best overlap rate on all four test sequences.

The proposed CM-ASS algorithm can successfully locate the target and the tracking results are close to the true value curve, as shown in Figure 6. This is mainly attributed to the effectiveness of the adaptive selection mechanism. The proposed adaptive selection mechanism detects the degradation of SDM and SGM by a distance metric strategy and temporarily discards the degraded model to construct a more reasonable likelihood function to evaluate the candidate samples of the current frame, thus effectively avoiding the introduction of inaccurate evaluation results that lead to error accumulation.

The sparse generative model effectively combines L_1 regularization and subspace representation to handle outliers while retaining sufficient representational power, aiming to

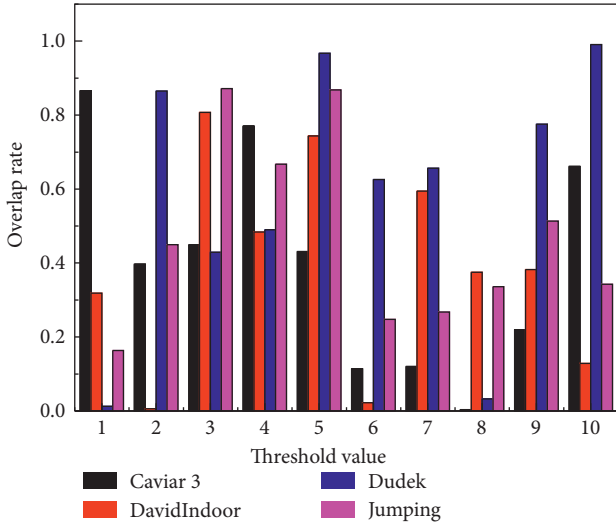


FIGURE 5: Overlap rate of different threshold algorithms on four test sequences.

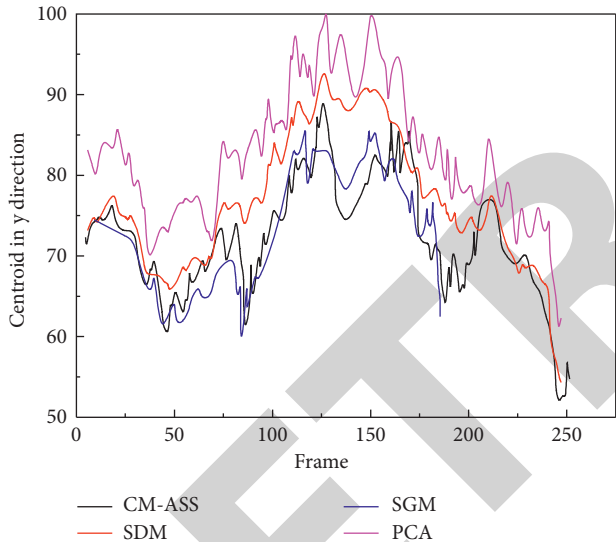


FIGURE 6: Comparison of trace results on sequences.

better portray the changes in target appearance. More importantly, this paper proposes a novel adaptive selection mechanism based on Euclidean distance to construct a more reasonable evaluation function, which overcomes the shortcomings of the traditional multiplicative fusion mechanism and can improve the overall performance of the joint model-based target tracking algorithm. And the adaptive selection mechanism is used to combine the sparse discriminative model and the sparse generative model organically under the framework of Bayesian citation. Also, different online update strategies are adopted for the template set and PCA subspace to mitigate the drift problem while ensuring that the algorithm can adapt to the changes of the tracking environment and target state. The experimental part compares with several classical or innovative tracking algorithms by both quantitative and qualitative analysis and proves that the proposed algorithm has a more robust tracking effect.

4.2. Video Analysis Results. Figure 7 illustrates the confusion matrix of the MCRL model on the MSR Daily Activity dataset. It can be seen from the figure that the proposed algorithm achieves a 100% recognition rate in 11 behavior categories. The larger error results occur in the confusion of the two behaviors play the game and sit still, potentially because the motion trajectories and contextual information of these two behaviors are highly similar.

Figure 8 shows the convergence profile of the MCRL model on the MSR Daily Activity dataset, which records the value of the objective function after each iteration of optimization. From the figure, 30 iterations are sufficient to obtain a reliable solution. Also, it is found that the proposed algorithm converges to a minimum after a finite number of iterations in all the experiments conducted in this paper. The algorithm is implemented in Matlab R2014a, and all experiments are performed on a computer configured with a 3.3 GHz Intel i5-4590 CPU and 8 G RAM. The computational speed of the proposed algorithm is about 0.36 sec/frame when extracting multimodal low-level features such as GJF, LDD, and LCD. For the training phase of the MCRL model, the algorithm runs in about 8.82 seconds/sample. The computation speed in the test phase is quite fast, spending about 16.05 ms for one sample. Also, Figure 8 gives the running times of different RGB-D behavior recognition algorithms on the MSR Daily Activity dataset for comparison. It can be seen that although the recognition rate of the proposed MCRL model is 0.62% lower than that of the JOULE model, the running time of the MCRL model is 8.6 times and 31.3 times faster than that of the JOULE model in the training and testing phases, respectively. This is because the MCRL model uses only three modal features, while the JOULE model incorporates six low-level heterogeneous features, which significantly increases the time overhead of the algorithm.

Usually, when the value of k is very small, the MCRL model is not sufficient to capture the complex relationships between multimodal data, and it tends to learn only a small fraction of the shared semantic structure between different modalities, resulting in poor performance of the algorithm. The recognition rate improves significantly when the value of k is gradually increased. This is because the MCRL model can capture the potential semantic connections among multimodal data and mine the shared features with strong differentiation for classification. At the same time, this also indicates to some extent that the original high-dimensional feature space contains a large amount of redundant information. The performance of the algorithm tends to stabilize as the value of k continues to get larger, indicating that the MCRL model starts to be insensitive to changes in the subspace dimension k . The potential reason for this is that the shared features learned from the MCRL model have captured enough discriminative information for classification.

Based on the empirical observation that the same human motion semantic information exists between different modal data, an MCRL model is proposed to learn shared features between multimodal data for classification. The original multimodal low-level features are first mapped to a compact

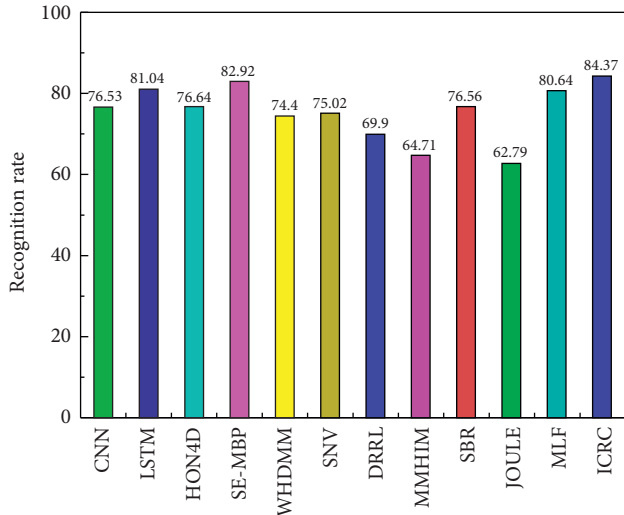


FIGURE 7: Comparison of algorithms with existing research work.

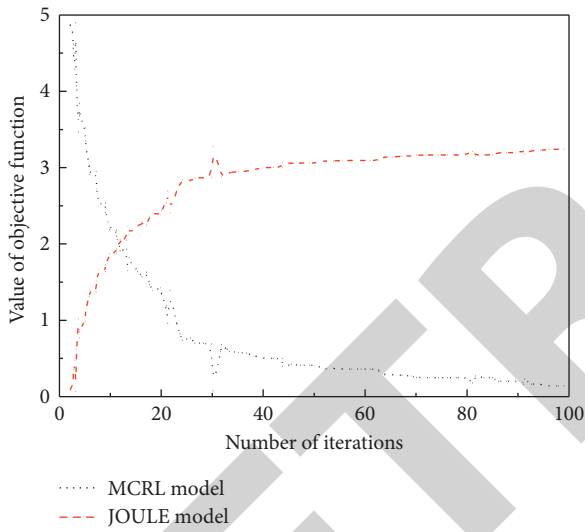


FIGURE 8: Convergence graph.

low-dimensional subspace, and then shared semantic features with distinguishing properties are mined in the subspace. The low-dimensional subspace and shared features are jointly learned by formulating an improved multitask learning framework. An iterative optimization algorithm is proposed to solve the model and obtain the optimal model parameters. Finally, an improved collaborative representation classifier based on a weight regularization matrix is used to accomplish fast behavior classification. Experimental results on four RGB-D behavioral datasets validate the effectiveness of the proposed algorithm in this chapter.

5. Conclusion

An adaptive Gaussian incremental expectation-based target tracking algorithm is proposed. The sparse generative model is constructed to retain sufficient appearance information while effectively resisting the interference of outliers and better portraying the appearance changes of the target itself.

To overcome the shortcomings of the traditional multiplicative fusion mechanism, an adaptive selection mechanism based on Euclidean distance is proposed, aiming to detect deteriorating models in time during the tracking process and adopt corresponding strategies to construct a more reasonable likelihood function. Based on the particle filtering framework, the adaptive selection mechanism is used to combine the sparse discriminative model and the sparse generative model. To mitigate the drift problem and ensure that the algorithm can adapt to the changing appearance of the target, different online updating strategies are adopted for the template set and the PCA subspace. Our results obtained a higher efficiency compared to other results, with an improvement of nearly 20% and a stronger accuracy, with an improvement of about 10%, and the algorithm has a strong practical value. The good robustness of the proposed algorithm is demonstrated through experiments on challenging test sequences and comparative analysis with several classical or innovative tracking algorithms. Also, an iterative optimization algorithm is proposed to solve the proposed model and obtain the optimal model parameters. The effectiveness of the proposed algorithm is verified by extensive experimental results on four RGB-D behavioral datasets and comparative analysis with existing innovative algorithms. It is worth mentioning that the experimental results show that the proposed model can transfer useful information learned from the training samples to the test samples, thus effectively coping with the situation where some modal data are missing in the test phase.

Data Availability

The data used to support the findings of this study are available from the corresponding author upon request.

Conflicts of Interest

The authors declare that they have no conflicts of interest in this paper.

References

- [1] A. Graser, P. Widhalm, and M. Dragaschnig, "The M^3 massive movement model: a distributed incrementally updatable solution for big movement data exploration," *International Journal of Geographical Information Science*, vol. 34, no. 6, pp. 2517–2540, 2020.
- [2] P. P. Roy, P. Kumar, and B. G. Kim, "An efficient sign language recognition (SLR) system using camshift tracker and hidden Markov model (HMM)," *SN Computer Science*, vol. 2, no. 2, pp. 1–15, 2021.
- [3] S. Tao, Z. Lei, and J. Chenkai, "Multi-frame moving video detection algorithm for IOT based on Gauss Monte Carlo particle filter," *International Journal of Computers and Applications*, vol. 42, no. 15, pp. 260–265, 2018.
- [4] P. R. Kamble, A. G. Keskar, and K. M. Bhurchandi, "Ball tracking in sports: a survey," *Artificial Intelligence Review*, vol. 52, no. 3, pp. 1655–1705, 2019.
- [5] S. Fu and N. Bouguila, "A soft computing model based on asymmetric Gaussian mixtures and Bayesian inference," *Soft Computing*, vol. 24, no. 7, pp. 4841–4853, 2020.

- [6] S. Zhang, J.-B. Huang, J. Lim et al., "Tracking persons-of-interest via unsupervised representation adaptation," *International Journal of Computer Vision*, vol. 128, no. 1, pp. 96–120, 2020.
- [7] A. A. Suman, M. N. Aktar, M. Asikuzzaman, A. L. Webb, D. M. Perriman, and M. R. Pickering, "Segmentation and reconstruction of cervical muscles using knowledge-based grouping adaptation and new step-wise registration with discrete cosines," *Computer Methods in Biomechanics and Biomedical Engineering: Imaging & Visualization*, vol. 7, no. 1, pp. 12–25, 2017.
- [8] E. Babae, N. B. Anuar, A. Wahid, S. S. Band, and A. T. Chronopoulos, "An overview of audio event detection methods from feature extraction to classification," *Applied Artificial Intelligence*, vol. 31, no. 9–10, pp. 661–714, 2017.
- [9] M. Xu, C. Li, Z. Chen, Z. Wang, and Z. Guan, "Assessing visual quality of omnidirectional videos," *IEEE Transactions on Circuits and Systems for Video Technology*, vol. 29, no. 12, pp. 3516–3530, 2019.
- [10] L.-C. Chen, "Improving the performance of Wikipedia based on the entry relationship between articles," *Journal of Internet Technology*, vol. 19, no. 3, pp. 711–723, 2018.
- [11] N. Koganti, T. Shibata, T. Tamei, and K. Ikeda, "Data-efficient learning of robotic clothing assistance using Bayesian Gaussian process latent variable model," *Advanced Robotics*, vol. 33, no. 15–16, pp. 800–814, 2019.
- [12] M. Jia, Z. Zhao, L. Huo, H. Chen, and Y. Qiu, "Incorporating global-local a priori knowledge into expectation-maximization for SAR image change detection," *International Journal of Remote Sensing*, vol. 40, no. 2, pp. 734–758, 2018.
- [13] S. Anthwal and D. Ganotra, "An overview of optical flow-based approaches for motion segmentation," *The Imaging Science Journal*, vol. 67, no. 5, pp. 284–294, 2019.
- [14] J. Bian, D. Tian, Y. Tang, and D. Tao, "Trajectory data classification," *ACM Transactions on Intelligent Systems and Technology*, vol. 10, no. 4, pp. 1–34, 2019.
- [15] A. Patel and J. Shah, "Sensor-based activity recognition in the context of ambient assisted living systems: a review," *Journal of Ambient Intelligence and Smart Environments*, vol. 11, no. 4, pp. 301–322, 2019.
- [16] A. Kubo, K. Meshgi, and S. Ishii, "A meta-Q-learning approach to discriminative correlation filter based visual tracking," *Journal of Intelligent & Robotic Systems*, vol. 101, no. 1, pp. 1–11, 2021.
- [17] X. Chen, K. Irie, D. Banks, R. Haslinger, J. Thomas, and M. West, "Scalable Bayesian modeling, monitoring, and analysis of dynamic network flow data," *Journal of the American Statistical Association*, vol. 113, no. 522, pp. 519–533, 2018.
- [18] C. Chen, F. Shen, J. Xu, and R. Yan, "Probabilistic latent semantic analysis-based gear fault diagnosis under variable working conditions," *IEEE Transactions on Instrumentation and Measurement*, vol. 69, no. 6, pp. 2845–2857, 2020.
- [19] D. Ramachandram and G. W. Taylor, "Deep multimodal learning: a survey on recent advances and trends," *IEEE Signal Processing Magazine*, vol. 34, no. 6, pp. 96–108, 2017.
- [20] C. Zhang, J. Cheng, L. Li, C. Li, and Q. Tian, "Object categorization using class-specific representations," *IEEE Transactions on Neural Networks and Learning Systems*, vol. 29, no. 9, pp. 4528–4534, 2018.
- [21] B. Bai, Z. Guo, C. Zhou, W. Zhang, and J. Zhang, "Application of adaptive reliability importance sampling-based extended domain PSO on single mode failure in reliability engineering," *Information Sciences*, vol. 546, pp. 42–59, 2021.
- [22] H. J. Ma and G. H. Yang, "Adaptive fault tolerant control of cooperative heterogeneous systems with actuator faults and unreliable interconnections," *IEEE Transactions on Automatic Control*, vol. 61, no. 11, pp. 3240–3255, 2016.
- [23] H. J. Ma and L. Xu, "Decentralized adaptive fault-tolerant control for a class of strong interconnected nonlinear systems via graph theory," *IEEE Transactions on Automatic Control*, p. 1, 2020.
- [24] J. Wen, J. Yang, B. Jiang, H. Song, and H. Wang, "Big data driven marine environment information forecasting: a time series prediction network," *IEEE Transactions on Fuzzy Systems*, vol. 29, no. 1, pp. 4–18, 2021.